Chiang Mai J. Sci. 2016; 43(6) : 1223-1236
http://epg.science.cmu.ac.th/ejournal/
Contributed Paper

From Mountain Heights to Basin Depths: The Importance of Thermal Geophysics in Tectonics, Seismology, and Petroleum Geoscience

Kevin P Furlong*
Department of Geosciences, Pennsylvania State University, University Park, PA USA 16802.
* Author for correspondence; e-mail: kpf1@psu.edu

Received: 30 June 2016
Accepted: 8 September 2016

ABSTRACT

Temperature conditions in the crust control many geologic processes. Careful incorporation of the thermal field can provide additional constraints on geologic and geophysical analyses. The basics of crustal and lithospheric thermal structure are discussed and two examples of application of thermal modeling for mountain building and basin evolution are provided.

Keywords: heat flow, geotherm thermochronology

1. INTRODUCTION

The thermal structure of the crust and lithosphere plays a critical role in constraining the nature of deformation and driving a range of key processes of geophysical relevance. For example, the maximum depth at which most earthquakes initiate and the characteristics of how strain accumulates during the earthquake cycle are very temperature dependent. Similarly, on a larger scale, lithospheric deformation, mountain building, and basin formation all are strongly controlled by the thermal regime - and as a result records of thermal history can allow this evolution to be quantified. Many physical properties of the crust and lithospheric mantle such as the seismic velocity, resistivity, density, and viscosity are strong functions of temperature, and thus knowledge of the thermal field are critical to appropriately interpreting geophysical measurements that reflect these properties. Finally, the conversion of raw organic material into economic hydrocarbon products such as oil and natural gas occurs through processes that are strongly temperature dependent; and in particular in the 80°C - 150°C range.

This general importance of understanding the thermal structure of the crust for geophysical studies motivates this report, which provides an overview of both crustal thermal structure and basic applications to processes of geophysical relevance. I will first provide background on the nature of the temperature structure and follow that with some specific examples of applications.

Thermal Structure of the Crust and Upper Mantle

The standard geotherm (temperature vs depth) model for the continental crust is generally produced using a one-dimensional, steady-state heat conduction equation in which the surface heat flow is in equilibrium with heat flowing into the lithosphere at its base plus the radiogenic heat produced within the lithosphere. I extend the geotherms only to the base of the lithosphere, a depth which seldom exceeds 250 km and over most of the Earth is much less. Throughout the lithosphere, heat production A varies with depth; thermal conductivity k varies with composition and with both pressure and temperature. Analytic solutions for geotherms T(z) exist when heat production follows some simple analytical forms and when thermal conductivity is constant or temperature dependent [1], however these requirements can be restrictive. In the results shown here we rather use an algorithm that breaks the lithosphere into layers with constant properties that can vary from layer to layer. The thickness of each layer can be made sufficiently small to represent complicated and discontinuous distributions of A(z) and k(z), for example 0.1 km.

The solution to the steady-state, one-dimensional heat conduction equation in a layer of constant heat generation A and constant thermal conductivity k is

$$T(z) = T_t + (q_t/k)\, z - (A/2k)\, z^2$$

where T_t and q_t are the temperature and heat flow respectively at the top of the layer and z is depth within the layer. If the layer has thickness Δz then the temperature at, and heat flow through, the bottom of the layer (T_b, q_b) are expressed in terms of the temperature and heat flow at the top of the layer (T_t, q_t) and properties (A,k) of the layer:

$$T_b = T_t + (q_t /k)\, \Delta z - (A /2k)\, \Delta z^2$$

and

$$q_b = q_t - A\Delta z$$

A geotherm T(z) is produced by applying these equations to successive layers, resetting T_t and q_t at the top of each new layer with the values T_b and q_b solved for the bottom of the previous layer. Thermal conductivity effects k(z, T) can also be incorporated and updated at each step in an iterative loop.

The overall pattern of thermal conductivity in the lithosphere is controlled by composition, temperature and, to a minor degree, pressure. The generalized lithosphere model used here consists of an upper crust of granite to andesitic composition, a lower crust consisting of gabbro or granulite facies metamorphic rock and an ultramafic upper mantle.

Compilations of thermal conductivity [2, 3] on several thousand rock samples provide a convenient summary from which an appropriate crustal thermal conductivity profile may be constructed. A value of 3.0 W m^{-1} K^{-1} represents a granitic upper crust for room temperature at which conductivities were measured. Lower crustal rock thermal conductivity is guided by averages for diorite (2.9 W m^{-1} K^{-1}), gabbro (2.6 W m^{-1} K^{-1}) amphibolite (2.5 W m^{-1} K^{-1}) and gneiss (2.4 W m^{-1} K^{-1}); we use 2.6 W m^{-1} K^{-1}, again assigned at room temperature.

Thermal conductivity at crustal conditions varies inversely with temperature and directly with pressure or depth according to the relation

$$k\,(T,z) = ko\,(1 + c\,z)/(1 + b\,(T\text{-}20))$$

where ko is the laboratory value, T is temperature in degrees Celsius, and b and c are constants. For the upper crust we use a temperature coefficient b of 1.5 × 10 -3 K^{-1}, intermediate for experimentally determined values for granite and granodiorite. For the lower crust, a temperature coefficient b of 1.0×10^{-4} is used. A pressure coefficient c of 1.5×10^{-3} km^{-1} is used throughout the crust. Zero depth and room temperature conductivities ko are 3.0 and 2.6 W m^{-1} K^{-1} for the upper and lower crust respectively. For the mantle, the model of Hasterok and Chapman [4] based on mantle compositions [5] and the peridotite lattice and radiative conductivities are used.

Surface heat flow reflects the combination of heat introduced from the underlying (and heat advecting) mantle into the conductive lid - the lithosphere - and heat generated within the lithosphere, primarily within the continental crust. The major producer of this crustal heat is radiogenic heat production, with the concentration of the heat producing materials in the crust varying with composition, metamorphic grade and in other less systematic ways. In spite of this inherent variability, observations of systematic behavior between observed surface heat flow and near-surface heat production are found for many geologic provinces. Specifically Birch et al [6] and Roy et al. [7] defined a series of heat flow provinces in which a linear relation between observed surface heat flow and heat production is seen. These heat flow provinces were defined as regions for which the observations satisfied a simple equation:

$$q_0 = q_r + b\,A_0$$

Where q_0 is observed surface heat flow, A_0 is a representative value for near-surface heat production in the vicinity of the observed heat flow and q_r and b are the linear regression parameters, with q_r representing the intercept at $A_0 = 0$, and b the slope of the regression line. There is significant scatter in such regressions, but, in general, the slope (b) of the regressed line, which has units of length, is typically in the 10-15 km range. This regression result is normally interpreted to reflect the two components of surface heat flow - q_r representing the heat flow into the base of the system (the Moho?, the base of the lithosphere?) and the length scale b related to the depth distribution of the heat production. Any arbitrary distribution that integrates to $b\,A_0$ is allowable, but initially three depth distributions were proposed [6, 7, 8]: (1) constant heat production A_0 over depth b and minimal heat production below that depth; (2) linearly decreasing heat production over depth $2b$, with surface value A_0 and base value 0; and (3) and exponentially decreasing value of heat production from a surface value of A_0 and with a 1/e folding length scale of b. All of these distributions lead to straightforward mathematical formulae for temperature-depth functions, and all are consistent with the observations that rocks comprising the upper crust typically have higher values of heat production than lower crustal and/or higher grade metamorphic rocks. Only the exponentially decreasing model [8] holds independently of exhumed crustal level.

The arguments that the exponential distribution best fits with concepts of crustal structure and evolution even led to numerous observational attempts to directly observe this exponential decrease with depth in exposed crustal sections. Although observed crustal sections showed that deeper (lower) crustal rocks were less radiogenic than shallower (upper) crustal rocks, that there was no systematic exponential distribution e.g [9, 10].

Geotherm models, the equations describing temperature as a function of depth, are generally one-dimensional in space. The assertion that the exponential depth distribution model produces the linear q-A relation in regions of differential erosion is strictly only true in the 1-D case. In many of the regions defined as heat flow provinces, crustal structure is not one-dimensional (i.e. not simply layered), but rather the crust is made of a mix of igneous and metamorphic bodies of varied dimensions and orientations. Two studies assessed the role that 3-D crustal structure and a heterogeneous distribution of heat production can play in observed surface heat flow behavior [11, 12]. Both studies modeled the result of crustal structure (either stochastic [12] or representative of observed crustal structure [11] , and came to similar results. When 2-D or 3-D heat transfer effects are included, the q-A relation results, with the length scale, *b*, related to the characteristic length scale of the crustal heterogeneity. The result is that the observed q-A relation seen in many regions most likely represents a partitioning of heat flow into a basal heat flow (q_r) representing the average heat flow at depth *b* in the crust, combined with the additional heat flow produced in the upper *b* km of the crust integrated over depth *b*.

Where does this leave the observed q-A relation and our ability to estimate lithospheric temperature structure? In most cases, crustal structure is not well enough imaged that precise modeling of temperature structure can be done. Rather the use of simple (but constrainable) geotherm models (such as using the exponential depth distribution for heat production), with suitable reference to the associated uncertainties is a reasonable approach. Although the lower crust is most often more depleted in heat producing elements than typical upper crust, assumptions of near-zero contributions to the crustal heat flow from heat production in the lower crust will lead to overestimates of mantle lithosphere heat flow and temperatures.

A family of continental geotherms for stable continental lithosphere, parametric in surface heat flow is shown in Figure 1. Temperature differences at a common depth between these bracketing geotherms can be large, ~ 500 K at 30 km depth and a maximum of 800 K at 60 km depth. One must recognize the diversity of temperature states available for different regions of the continental lithosphere and, for any application, seek the most appropriate region for a particular region of interest.

Also shown on Figure 1 are representative solidii curves for the crust [13]. The hottest thermal states characterized by the 80 and 90 mW m^{-2} geotherms could provide for deep crustal melting under hydrous conditions; dry melting in the crust seems to be precluded in regions where these steady-state, static geotherms apply. The accepted P-T field for metamorphism is also shown on Figure 1. Lack of complete overlap between the geotherms and metamorphic P-T space requires dynamic tectonic processes such as subduction (low T, high P) or magmatic processes (high T, low P) which can be considered as perturbations to the framework geotherms.

Thermal Constraints on Tectonic-Geophysical Processes

A very wide range of tectonic and geophysical processes are both affected by and record the interactions between deformation and the thermal regime. Here I provide two examples of the application of thermal modeling (in conjunction with geochemical and geochronological systems) to define the tectonic regimes. In the first, the use of relatively low-temperature thermo-chronology systems (~60°C - ~300°C) allows us to place significant constraints on the rates of uplift and fault slip on the major faults in the vicinity of the 2008 Wenchuan (China) earthquake. In the second, I illustrate how modeling of the thermal structure in conjunction with analyses of the levels of organic maturation in a petroleum prospect can place limits on the timing and rates of plate subduction.

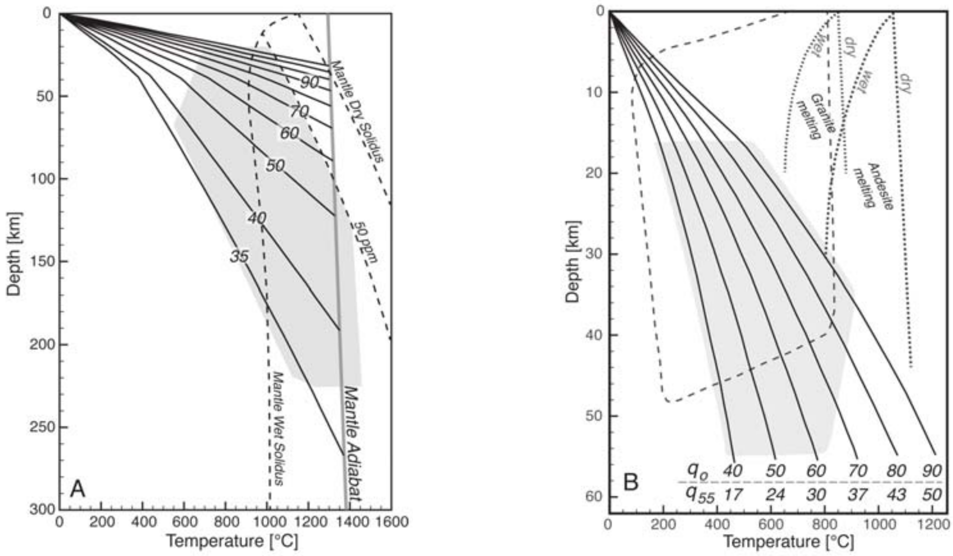

Figure 1. A. Lithospheric scale geotherms for continental regions parameterized by surface heat flow q_o. (labeled on each curve in mW/m^2, unlabeled curves are the 80, 100, 110, and 120 mW/m^2 geotherms). Mantle 1300 °C adiabat is shown by labeled grey line. Melting conditions (solidus) from Katz et al. [28] for dry and hydrous conditions are indicated. Shaded region represents P-T estimates for nearly 1500 mantle xenoliths (see [4] for discussion). Heat production for geotherms varies with depth and in the upper crust with surface heat flow. In the upper crust Heat Production (A) is selected to produce a reduced heat flow at the base of the upper crust that is 26% lower than the observed surface heat flow (i.e. q_o/q_r = 0.74).

B. Crustal scale geotherms for continental regions parameterized by surface heat flow q_o, Difference between heat flow at the surface (q_o) and at a depth of 55 km (q_{55}) is supplied by crustal heat production. Crust is assumed to be 35 km in thickness. Dashed lines labeled granite and andesite show possible solidii brackets for hydrous (wet) and dry melting in the crust. Shaded polygon encloses steady-state Depth (P)-T field of lower crust in stable regions. Dashed line encloses Depth (P)-T field appropriate for metamorphic rocks. The lack of overlap in temperature-depth space between stable temperature conditions and some of the range of metamorphic conditions can be ascribed to dynamic tectonic processes.

Longmen Shan Uplift

In 2008, a Mw 7.9 earthquake occurred primarily along the Yingxiu-Beichuan Fault in Sichuan Province, China. This was an extremely deadly and damaging earthquake, and its occurrence raised significant questions about the rates of fault motion and the overall tectonic setting of this obliquely converging set of crustal faults. The example and interpretation provided here are based on the results of Wang et al. [14]. As a result of ongoing shortening across the Longmont Shan region there is significant uplift with resulting extreme topographic relief (Figure 2).

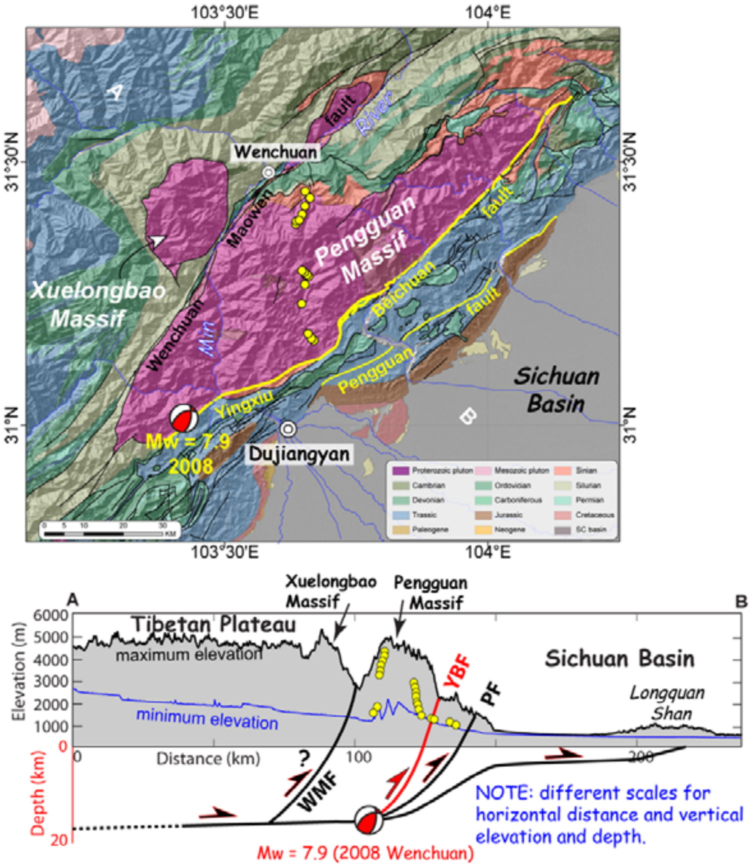

Figure 2. A. Simplified geologic map of the plateau margin adjacent to the Sichuan Basin in the Longmen Shan. Sample locations are shown for the age-elevation transect in the Pengguan Massif ([14]; yellow circles). Yellow lines show the faults that ruptured in the 2008 Wenchuan earthquake. B. Simplified cross-section showing the topographic and structural position of the transect, as well as inferred crustal fault geometry.

We collected a suite of samples spanning more than 3000 meters in elevation and determined both Fission Track and (U-Th)/He ages for both Apatites and Zircons (AFT, AHe and ZFT, ZHe respectively) within the samples. Each of these thermochronologic systems provide information about the timing when the samples were in specific temperature conditions. ZFT ages reflect Temperatures of ~ 350°C-250°C; ZHe ~ 180°C; AFT ~ 120°C: and AHe ~ 60°C. With this wide range of temperatures being recorded this suite of data can provide information of uplift and unrolling from the middle crust to very near the surface. Age results from these samples are shown in Figure 3. All of the samples showed ZFT ages that were ~ 200 Ma or greater and thus indicate that all samples were shallower/cooler than ~ 250°C since that time. However all other systems shows ages younger than ~ 60 Ma at all levels indicating that they reflect tectonic activity over the period from ~ 60 Ma to the Present.

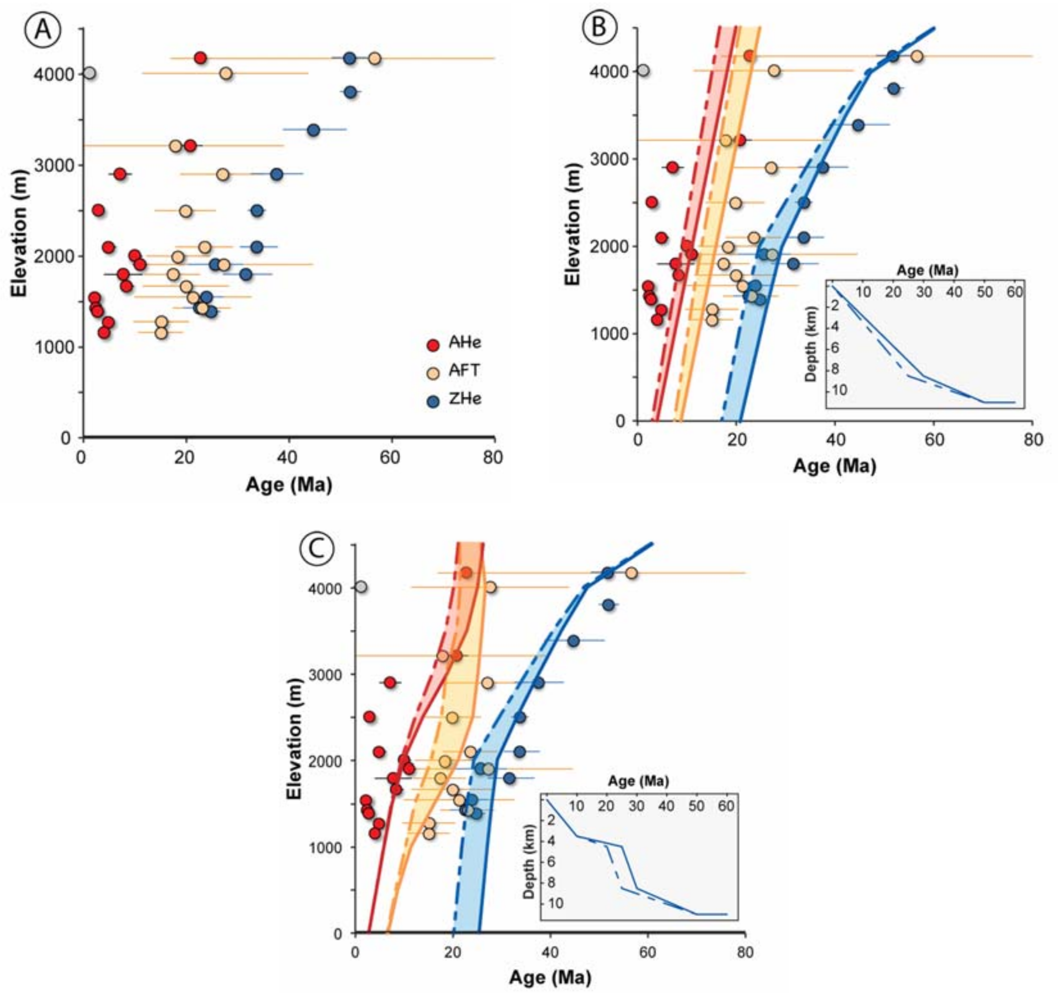

Figure 3. A. Low-temperature thermochronometric results from an age-elevation transect in the Pengguan Massif (Figure 2) showing zircon (U-Th)/He (ZHe), apatite fission-track (AFT) and apatite (U-Th)/He (AHe) determinations [14]. B. Results of thermal models representing a single-stage rapid exhumation event starting in Late Oligocene (solid) and Early Miocene (dashed) time and continuing to present (inset shows depth-time history of model). Note that this scenario does not explain AFT or AHe data very well. C. Two-stage exhumation history that requires a ~10 Ma hiatus in exhumation during Early Miocene time [14].

We can use the time-temperature history record in these samples to infer the uplift (cooling) history of the region of the Pengguan Massif within the Longmen Shan. The results of that modeling and the fit to the observed data are shown in Figure 3. Within the uncertainties in the data, we can bracket the uplift/cooling history as shown in the figure. Of particular importance is the requirement from the modeling results that there be two intervals of relatively rapid uplift (~30-20 Ma and ~10 Ma to Present) separated by and interval of little-to-no uplift and unroofing. This punctuated nature for the uplift may imply a complex interplay among the tectonics processes that are driving shortening and uplift along the eastern margin of the Tibetan Plateau.

Subduction Initiation and Hydrocarbon Maturation

Hawke's Bay Basin, along the Hikurangi Subduction Margin on East Coast of New Zealand's North Island, underwent a transition from crustal extension to crustal shortening and subduction over the past 40 Ma [15] (Figure 4). The thermal signatures of both crustal extension and convergence have had a significant impact on the thermal evolution and associated maturation of hydrocarbon source rocks in the basin. Here we use proxies for temperature history including Apatite Fission Track (AFT) thermochronology and vitrinite reflectance (R_o) recorded in the Opoutama-1 well to constrain the timing and thermal effects of extension and subduction along the Hikurangi Margin.

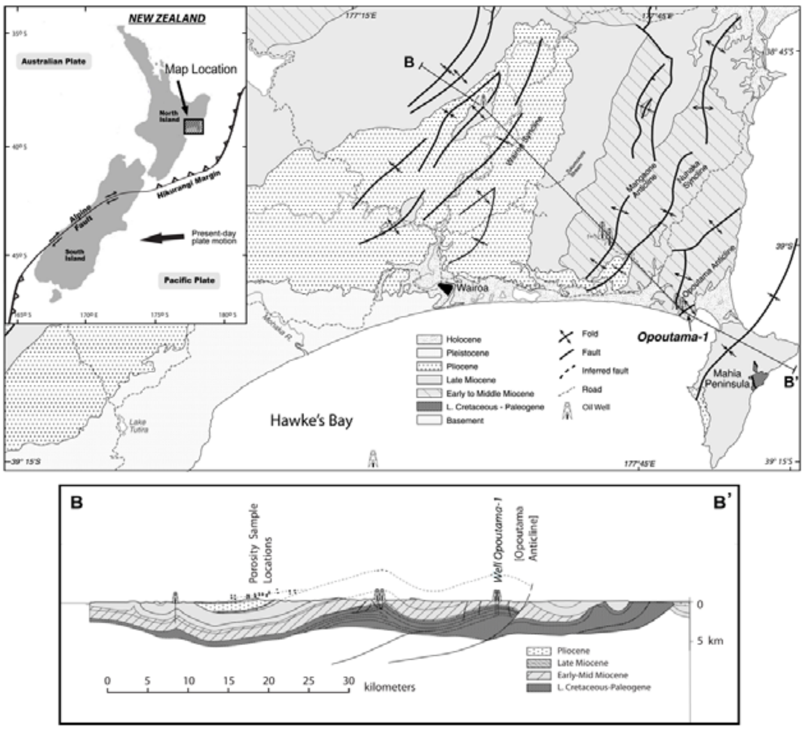

Figure 4. Structural Geologic Map of Hawke's Bay. Well Opoutama-1 sits on the Opoutama Anticline on the Mahia Peninsula, through which cross-section A-A' is drawn. Hawke's Bay Synclines and anticlines are reflective of ongoing convergence and subduction along the Hikurangi Margin, and are considered to be the most promising structural hydrocarbon traps in Hawke's Bay. The upper-righthand corner inset is generalized map of New Zealand showing the location of Hawke's Bay, the Australian-Pacific plate boundary, and a thick black arrow indicating the present oblique-convergent motion of the Pacific Plate with respect to the Australian Plate. Cross-section B-B' (modified from [24]) is a schematic of the structures in Hawke's Bay with generalized lithologies. Well Opoutama-1 was drilled at the crest of the Opoutama Anticline to a total depth of 3.66 km.

Hawke's Bay Basin records a depositional history since 95 Ma. The Whangai, Waipawa, Wanstead, and Weber Formations represent the deposition of low-energy mudstone from ~95-25 Ma. Of these, the Whangai has been considered to have the most hydrocarbon source potential of the units preserved in Opoutama-1 [16, 17], and has been the target for previous thermal and hydrocarbon maturation models.

The tectonic setting of the New Zealand region changed considerably during the period of deposition. Contemporaneous with deposition of these mudstones, New Zealand migrated away from Antarctica towards its present location with the breakup of Gondwanaland. Between ~ 40 Ma and 30 Ma, New Zealand underwent extension leading to subsidence of large areas of the continent, with substantial regions submerged at 30 Ma [18, 19]. Mudstone deposition in Hawke's Bay continued until ~16 Ma when the Tunanui sandstone was deposited, following the onset of subduction beneath Hawke's Bay Basin ~ 25 Ma (Figure 2). The Tunanui Fm. is a fine sandstone flysch, interpreted to result from uplift to the west associated with convergence along the Hikurangi Margin [17]. Subduction propagated South from 25 Ma-Present, thus the timing of subduction initiation varies along the present-day East Coast of North Island, New Zealand [19]. However the Hawke's Bay region is interpreted to have been along the leading edge of the continent [19] and thus underwent the transition to subduction early in the plate boundary evolution (~ 25-20 Ma).

Surface heat flow in the upper crust varies depending on tectonic setting. Regions undergoing extension, such as the modern-day Basin and Range province of North America, have relatively high heat flow. The average heat flow in continental crust is 65 mW m^{-2} ([20]), whereas surface heat flow values in the Basin and Range are 63-104 mW m^{-2} with an average of 85 +/- 10 mW m^{-2}. Therefore, when New Zealand was undergoing extension prior to 30 Ma, these elevated values are more appropriate to be applied in any modeling. Conversely, where subduction occurs, cold down-going lithosphere acts to cool the overlying crust, resulting in suppressed surface heat flow [21, 22]. This effect is amplified as the depth to the slab shallows. Along the Hikurangi Margin present-day heat flow values are around 30-40 mW m^{-2} at the trench, and between 40-50 mW m^{-2} at Hawke's Bay [23]. Corrected present-day heat flow at the Opoutama-1 well is 50 +/- 5 mW m^{-2}.

We use previously determined burial and exhumation histories (Figure 5) for the well-site [24, 17] to define a set of burial and erosion events for the modeling. We test various values of background heat flow, and also test the effects of subduction (varying timing of subduction initiation and depth of the subduction slab beneath the site) on the thermal history of specific units within the well for which we have data constraining apatite fission track (AFT) age and track length distribution [24] and vitrinite reflectance (Ro) values [25].

We model hydrocarbon production based on the thermal histories for each model scenario. We assume a type II kerogen since potential sources, including the Whangai fm., are marine siltstones and mudstones. Maximum production is assumed to be 630 mg/g, typical of type II kerogen [26]. Potential hydrocarbon production (and production rate) through time is determined at the depth of each AFT sample unit; in addition two additional stratigraphic levels are monitored, one and two kilometers below the present day bottom of the well.

Using a variety of data sets including Apatite Fission Track (AFT) ages and lengths, stratigraphy, present-day heat flow, and vitrinite reflectance (R_o). We evaluate possible burial/exhumation histories and assess the associated thermal histories of the upper crust in the Hawke's Bay Basin. Three model scenarios are presented to highlight different aspects of the thermal evolution of Hawke's Bay. The scenarios are: (a) Kamp and Xu [24] burial history, (b) same burial history but assumed higher heat flow, and (c) Elevated pre-25 Ma heat flow followed by subduction emplacement.

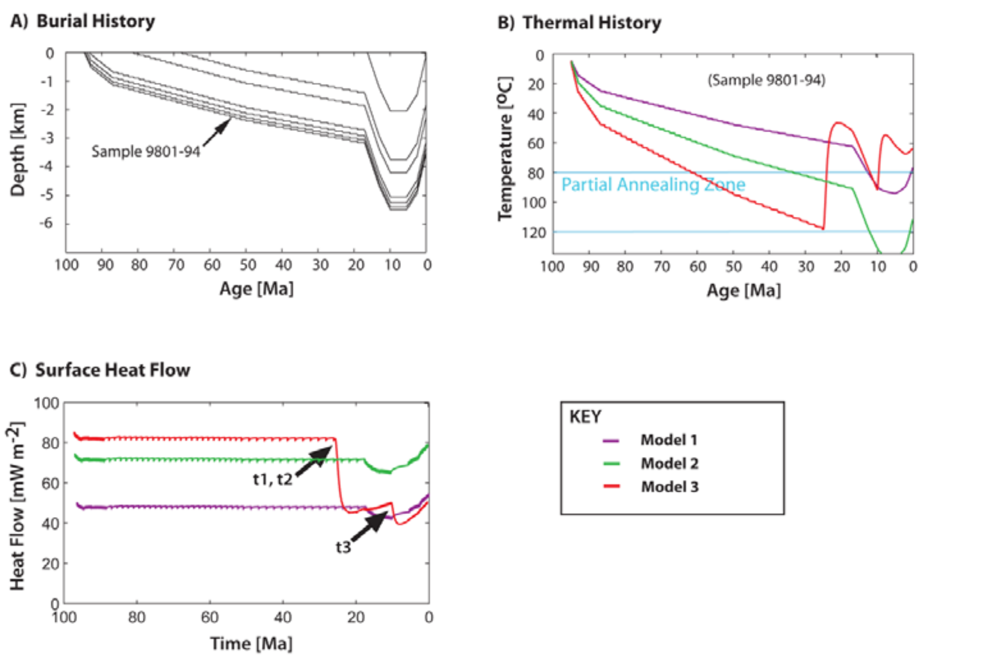

Figure 5. Burial and thermal histories for models shown here. All models have the same burial history and differ only in terms of background heat flow and/or inclusion of thermal effects of subduction. A. Burial histories. All models use burial history proposed by Kamp and Xu [24]. B. Resulting thermal histories (for representative unit) for three models. Model 1 uses present day heat flow (~ 50 mW m^{-2}) and no subduction effects; Model 2 uses elevated heat flow throughout duration of model (~ 75 mW m^{-2}); Model 3 uses elevated heat flow (~ 102 mW m^{-2}) during Eocene-Oligo one time to reflect period of extension and rifting, and incorporates effects of subduction. C. Resulting surface heat flow for each model.

The burial history of Kamp and Xu incorporates burial of each unit according to its biostratigraphic age as determined by Field and Uruski [17]. The four deepest samples enter the basin between 95-93 Ma and reach depths of ~ 2.5-3 km by 16 Ma, at which time the burial rate increases (Figure 5).These samples reach maximum depths > 5 km at 10 Ma. Exhumation occurs along shallow thrust faults from 7 Ma- present, bringing the samples to their present depths of ~ 3-3.6 km. Total depths of burial and amounts eroded (post-7 Ma) were determined from porosity measurements and the geometry of units mapped on the flanks of the Opoutama-1 anticline.

Initial surface heat flow (q_o) used for this model is 50 mW m^{-2}, which produces a modeled present-day value of 52 mW m^{-2}, in good agreement with the observed value of 50 +/- 5 mW m^{-2} [27].

The time-temperature history corresponding to this burial history and heat flow shows maximum temperatures being reached at 5 Ma, but not exceeding 100 °C. The four deepest Opoutama-1 samples enter the partial annealing zone at ~12 Ma, where they reside until they are cooled below 80 °C at ~ 1 Ma. Because no samples reach 120 °C, the upper limit of the partial annealing zone, none gets reset with respect to AFT; therefore all ages and length distributions for this model are the result of partial annealing and/or provenance signal. The four deepest AFT samples (AFT sample numbers 9801-94, 9101-7, 9801-93, 9801-91) have biostratigraphic ages of ~95-90 Ma; sample 9101-6 is dated to be ~82 Ma; sample 9101-5 is ~69 Ma; and sample 9101-4 is ~13 Ma (Figure 6).

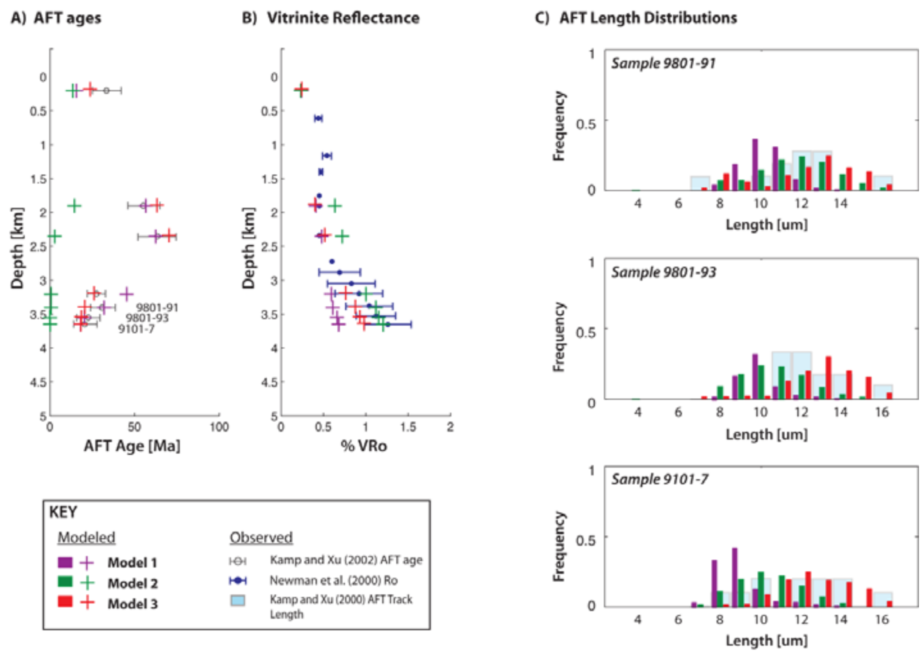

Figure 6. Comparison of models with and without effects of subduction. AFT ages, Vitrinite Reflectance, and AFT length distributions compared for the Kamp and Xu model without subduction, q_o = 50 mW m^{-2} (Model 1), Kamp and Xu without subduction, q_o = 75 mW m^{-2} (Model 2) and similar burial history but effects of rifting and subduction included (Model 3); Model 1 satisfies the AFT ages but not the R_o profile. Model 2 satisfies the R_o data but not the AFT ages. Model 3, which incorporates tectonic thermal effects, agrees with both the AFT ages and the R_o data, as well as producing the preferred match to the AFT length data.

Using the Kamp and Xu burial history, model AFT length distributions are on average too short (Figure 6), (Sample 9101-7 is omitted due to sparseness of observed lengths). Samples 9101-4, 9101-5, and 9101-6 are never hotter than ~90 °C in the model, thus their AFT signal is primarily provenance, having little record of events that took place post-deposition in the basin. Observed track length distributions for samples 9101-7, 9801-93, and 9801-91 all center on 12 microns, whereas modeled distributions center on 9, 10, and 11 microns respectively. The difference reflects a higher degree of annealing (i.e. higher temperatures for longer) in the model than observed in the samples. This model fails to predict the observed degree of thermal maturation (R_o) for the bottom four Opoutama-1 samples (Figure 6). For the deepest sample from the well this model produces R_o=0.86, substantially less mature than the R_o=1.26 observed by Newman et al. [25]. The model results for the three samples below 3 km depth similarly underestimate the maturation level.

In the model including effects of higher heat flow pre-Neogene and subduction initiation in the Early Miocene: 1) the upper crust has an initial surface heat flow of q_o = 102 mW m^{-2} prior to subduction emplacement to reflect evidence of regional extension/crustal thinning; and 2) a series of thrust events work to cool basin sediments, simulating subduction beginning at 25 Ma. We use the burial history of Kamp and Xu in this model, but with the elevated heat flow prior to 25 Ma and the thermal effects of subduction post-25 Ma, the resulting thermal history (Figure 5) looks markedly different from the thermal history in the Kamp and Xu model. Temperatures for these samples enter the partial annealing zone once again at ~11 Ma, but not long enough to produce enough annealing to significantly affect their AFT ages and track length distributions.

Heat flow for the model is ~ 102 mW m^{-2} from 100-25 Ma reflecting the effects of regional extension through the Eocene-Oligocene, and drops to ~ 40 mW m^{-2} by 23 Ma and remains below 50 mW m^{-2} until the present-day, reflecting the continued influence of the cold down-going slab. Model AFT ages cluster around the observed ages for the deepest four samples and the remaining samples fit the profile shape (Figure 6). Length distributions center on 12 and 13 microns for the three distributions shown (Figure 6), in much better agreement with the observed lengths, as compared to the Kamp and Xu model.

This model produces good agreement with R_o for the entire section (Figure 6), with the deepest sample reaching R_o=1.13 in the model. High heat flow prior to 25 Ma causes this trend, while the sudden drop in heat flow associated with subduction leads to a cooler geothermal gradient post-25 Ma and AFT ages reset to the 18-30 Ma range for the deepest four samples.

Potential hydrocarbon source rocks in Hawke's Bay include the Whangai Fm. (~85-65 Ma), Waipawa Fm. (~63 Ma), Wanstead fm (~55-35 Ma), and Weber Fm. (~35-25 Ma). Of these the Whangai Fm. alone has been identified in Opoutama-1 well, and exhibits the most economic hydrocarbon potential [16]. AFT sample 9101-5 corresponds to the Whangai Fm.

Using the Kamp and Xu burial history and a heat flow, q_o = 50 mW m^{-2} the Whangai Fm. has no significant hydrocarbon production. A source at the base of the well shows some production during the interval 10 Ma-present, and potential source mudstones at 4.7 km and 5.7 km depth show significant production from ~15 Ma-present. Using the Kamp and Xu burial history but with an elevated heat flow, q_o = 75 mW m^{-2}, the Whangai Fm. undergoes some hydrocarbon production in the interval 10 Ma-present, the base of Opoutama-1 experiences significant production from 15-10 Ma, and the 4.7 km- and 5.7 km-deep samples experience on-going oil generation from ~90-15 Ma. The low heat flow (q_o = 50 mW m^{-2}) model satisfies the AFT age data and the higher heat flow model (q_o = 75 mW m^{-2}) satisfies the R_o data, but neither satisfies both, nor does either adequately match AFT length distributions (Figure 6).

For the geologic history shown in Figure 5, with high pre-subduction heat flow and subduction initiation at ~ 25 Ma, the AFT age, AFT track length distribution and R_o observations in the well (Figure 6) are well matched. In terms of hydrocarbon production, the Whangai Fm. generates no significant hydrocarbons at any point in time, and production in deeper targets occurs almost entirely prior to subduction at 25 Ma. Therefore it is possible that little hydrocarbon generation has occurred contemporaneous with the formation of the Opoutama Anticline in the interval 7 Ma-present.

These model results indicate that the processes responsible for peak thermal maturation at Opoutama-1 occurred during a time of regional extension and high heat flow prior to 25 Ma, and that the processes responsible for structural trap formation in the shallower units (e.g. subduction/ convergence) occurred since the onset of subduction at 25 Ma. Since the extension and subduction modeled here are regional processes, it is possible that peak maturation predates Miocene and younger deformation throughout Hawke's Bay.

Discussion

The thermal regime for the crust is oftentimes a secondary consideration in geophysical studies; these examples show the importance it can play in interpretations of other geological, geochemical or geophysical data and processes. Careful incorporation of constraints provided by such thermal analyses can separate among various models of crustal development, provide an understanding of earthquake hazards, and can distinguish among different models of basin evolution, a crucial consideration in evaluating petroleum system prospects.

References

[1] Rybach L., Geothermal Systems, Conductive Heat Flow, Geothermal Anomalies; in Rybach L. and Muffler L.J.P., eds., *Geothermal Systems: Principles and Case Histories*, 1981: 3-36.

[2] Roy R.F., Beck A.E. and Touloukian Y.S., Thermophysical Properties of Rocks; in Touloukian Y.S. and Ho C.Y., eds., *Physical Properties of Rocks and Minerals,* Vol. II-2, New York: McGraw-Hill, 1981: 409-502.

[3] Cermak V. and Rybach L., Thermal Conductivity and Specific Heat of Minerals and Rock; in Angenheister G., ed., *Landolt-Bornstein Numerical Data and Functional Relationships in Science and Technology*, New Series. Group V. vol 16, Berlin, Springer-Verlag, 1982.

[4] Hasterok D. and Chapman D.S., *Earth Planet. Sci. Lett.*, 2011; **307**: 59-70.

[5] Griffin W., O'Reilly S. and Ryan C., The Composition and Origin of Sub-continental Lithospheric Mantle; in Fei Y., Bertka C. and Mysen B., eds., *Mantle Petrology: Field Observations and High Pressure Experimentation: A Tribute to Francis R. (Joe) Boyd,* Special Publication 6. Geochem. Soc., St. Louis, MO, 1999: 13-45.

[6] Birch F., Roy R. and Decker E., Heat Flow and Thermal History in New England and New York; in Zen E., et al., eds., *Studies of Appalachian Geology: Northern and Maritime,* Interscience, New York, 1968: 437-451.

[7] Roy R., Blackwell D. and Birch F., *Earth Planet. Sci. Lett.*, 1968; **5**: 1-12.

[8] Lachenbruch A., *J. Geophys. Res.,* 1970; **75**: 3291-3300.

[9] Fountain D., Salisbury M. and Furlong K., *Can. J. Earth Sci.*, 1987; **24**: 1583-94.

[10] Nicolaysen L.O., Hart R.J. and Gale N.H., *J. Geophys. Res.*, 1981; **86**: 653-661.

[11] Furlong K. and Chapman D., *Geophys. Res. Lett.*, 1987; **14**: 314-317.

[12] Nielson S., *Geophys. Res. Lett.*, 1987; **14**: 318-321.

[13] Myson B.O., Melting Curves of Rocks and Viscosity of Rock-forming Minerals; in Touloukian Y.S. and Ho C.Y., eds., *Physical Properties of Rocks and Minerals,* Vol. II-2, New York, McGraw-Hill, 1981; 361-407.

[14] Wang E., Kirby E., Furlong K.P., van Soest M., Xu G., Shi X., Kamp P.J.J. and Hodges K.V., *Nature Geosci.*, 2012; **5**: 640-645. DOI: 10.1038/NGEO1538.

[15] Furlong K.P. and Kamp P.J.J., *Tectonophysics*, 2013; **608**: 1328-1342. DOI 10.1016/j.tecto.2013.06.008.

[16] Davies E.J., Frederick J.B., Leask W.L. and Williams T.K., *New Zealand Petroleum Conference Proceedings*, 19-22 March 2000; 11.

[17] Field B.D. and Uruski C.I., Book: Cretaceous-Cenozoic geology and petroleum systems of the East Coast region, New Zealand, Monograph 19, Institute of Geologolical and Nuclear Sciences, Lower Hutt, New Zealand, 1997; 301.

[18] Landis C.A., Campbell H.J., Begg J.G., Mildenhall D.C., Paterson A.M. and Trewick S.A., *Geological Magazine*, 2008; **145**: 173-197.

[19] Furlong K.P. and Kamp P.J.J., *Tectonophysics*, 2009; **474**: 449-462.

[20] Pollack H.N., Hurter S.J. and Johnson J.R., *Rev. Geophys.*, 1993; **31**: 267-280.

[21] Henry S.G. and Pollack H.N., *J. Geophys. Res.*,1988; **93**: 15153-15162.

[22] Lewis T.J., Bentkowski W.H., Davis E.E., Hyndman R.D., Souther J.G. and Wright J.A., *J. Geophys. Res.*, 1988; **93**: 15207-15225.

[23] Henrys S.A., Ellis S. and Uruski C., *Geophys. Res. Lett.*, 2003; **30**: 1065.

[24] Kamp P.J.J. and Xu G., *New Zealand Petroleum Conference Proceedings*, 24-27 February 2002.

[25] Newman J., Eckerlsey K.M., Francis D.A. and Moore N.A., *New Zealand Petroleum Conference Proceedings*, 2000.

[26] Ungerer P. and Pelet R., *Nature*, 1987; **327**: 52-54

[27] Townend J., *Mar. Geol.*, 1997; **141**: 209-220.

[28] Katz R., Spiegelman M. and Langmuir C., *Geochem. Geophys. Geosyst.*, 2003; **9**: 1073.